Multi-Modular Isolated Three-Phase AC-DC Converter for Rapid Charging with Autonomous Distributed Control

Masakazu Adachi [1)] Keisuke Kusaka [1)] Jun-ichi Itoh [1)]

1) Nagaoka University of Technology, Electrical, Electronics and Information Engineering

1603-1 Kamitomioka-machi, Nagaoka, Niigata, 940-2188, Japan (E-mail: itoh@vos.nagaokaut.ac.jp)

Presented at EVS 31 & EVTeC 2018, Kobe, Japan, October 1 - 3, 2018

ABSTRACT: This paper proposes autonomous distributed control method for the multi-modular isolated three-phase AC-DC converter. Multi-modular topologies, which have multiple modules, are suitable for high voltage rapid charging of an onboard battery of electric vehicles. In conventional control for multi-modular topology, balance control with fast response must be employed by centralized controller. In the proposed method, the high-speed communication between the controller on each module and centralized controller is not needed because the input current and the output voltage is autonomously controlled by each distributed controller on the modules. As experimental results confirmed that the input current is balanced among the modules without high-speed response main controller.

KEY WORDS: Battery charging, Rapid charging, Autonomous distributed control, Power factor correction converter

1. INTRODUCTION

In recent years, charging power of rapid chargers for electric vehicles has been increasing[(1)-(6)]. Thus, the input AC voltage should be increased from the 100 V or 200 V in the present system to the medium voltage corresponding to the increase of charging power. However, in a conventional single-circuit topology, the volume of system and switching devices rapidly increases with the high voltage and the high charging power. For example, rapid chargers for electric vehicles is connected to 500 V according to the CHAdeMO association[(7)]. Thus, the volume of the transformer is bulky because the high transform ratio is required in order to convert from the grid voltage of 6.6 kV to several hundred volts.

As a solution to suppress volume of the circuit, multi-modular topology has been proposed because the multi-modular topology is suitable for medium or high voltage system and high-power converter[(8)-(9)]. The multi-modular topology has advantages that low-voltage-rating semiconductors are used. Moreover the multi-modular topology will improve power density through miniaturization of passive components because rated power per module is lowered in the multi-modular topology. In the conventional method, the three-phase voltage is separated into three separate phases. Each phase is independently controlled as a single-phase AC-DC converter. The multi-module single phase AC-DC converter is reduces the number of the switching devices compared to the multi-module three-phase AC-DC converter[(10)]. As described above, an unbalance of the three-phase input currents may occurs due to the error of detection gain of each module when each phase of the three-phase AC-DC converter is independently controlled. Thus, the multi-modular topology needs current balance control among each phase by centralized control, e.g., the master-slave control. Consequently, the conventional control method requires fast response for the communication among the master controller and the slave controller [(11)-(12)].

This paper proposes autonomous distributed control method for the isolated three-phase AC-DC converter in which a controller is included in each module. Therefore, the droop control is applied to the controller in order to stably control the input current of each phase[(13)-(15)]. The input current divergence is avoided by controlling the droop gain range to be larger than the detection error.

In addition, the current balance control is operated by averaging the input current amplitude of each phase. Thus, the autonomous distributed control is achieved by slow responses of the droop control and the current balance control without the

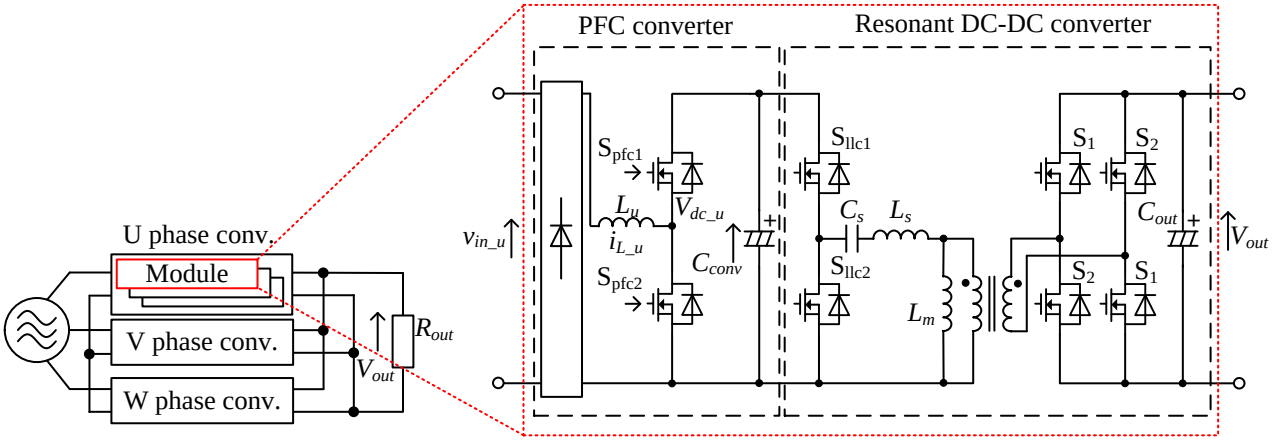

Fig. 1. Configuration of isolated three-phase AC-DC converter with autonomous distributed control.

mutual communication among each phase. Therefore, the main controller is needed only to have a function of the mutual communicating among each phase, whereas the high-speed control is performed in the module controller. As a result, wireless communication is used for communication among the main controller and each module controller.

This paper is organized as follows. In the second section the circuit configuration of the proposed isolated three-phase AC-DC converter is introduced. Then, a control method of the output DC voltage and the input current are described. In addition, the droop control and the current balance control, which are applied for balancing the currents of the modules, are shown.

In the second section shows the current imbalance rate when the droop control and the current balance control of an isolated three-phase AC-DC converter are applied. The current imbalance rate is reduced from 49.4% to 0.1% by adding the current balance control compared with only the droop control. Therefore, even when the imbalance occurs in the detection gain, it confirms that input current balance is achieved.

Finally, the experiment results shows that the sinusoidal input current and the balanced current share among each phase are achieved.

2. CONFIGURATION OF PROPOSED SYSTEM

2.1. Circuit configuration

Figure 1 shows the circuit configuration of the proposed isolated three-phase AC-DC converter. In the proposed circuit, control of a single-phase AC-DC converter is employed because each phase is independently controlled.

Each phase module consists of the power-factor-correction (PFC) converter and the resonant DC-DC converter. The PFC converter corrects the power factor to be unity and controls the input current to be sinusoidal. In this proposed circuit, a large capacitor is not needed, difference from the conventional PFC, because the power pulsation at the output is canceled by the phase difference of the three-phase alternating current by connecting the output of each phase in parallel. Therefore, the single-phase power pulsation at twice the grid frequency does not occur.

The resonant isolated DC-DC converter provides isolation between input and output. High frequency excitation and zero current switching (ZCS) are achieved by utilizing the series resonance between leakage inductance L_s of high frequency transformer and capacitor C_s connected to the primary side of the transformer. Each MOSFET of the high-frequency inverter switches at the zero current crossing points by matching the switching frequency to the resonance frequency.

As a result, switching loss is greatly reduced. The magnetizing inductance is designed to be sufficiently large compared to the leakage inductance. Therefore, the magnetizing inductance is negligible. The resonance frequency f_o is given by

$$f_o = \frac{1}{2\pi\sqrt{L_s C_s}} \quad (1).$$

As described above, in order to achieve turn-on and turn-off ZCS, the switching frequency of the resonance DC-DC converter is set to be equal to the resonance frequency, and the resonance isolated DC-DC converter is operated in open loop with a duty ratio of 50%.

2.2. Control block diagram

Figure 2 shows the control block diagram. The control of the proposed circuit consists of several module controllers and the main controller. In the module controllers, automatic output voltage regulator (AVR) and automatic input current regulator (ACR) are implemented.

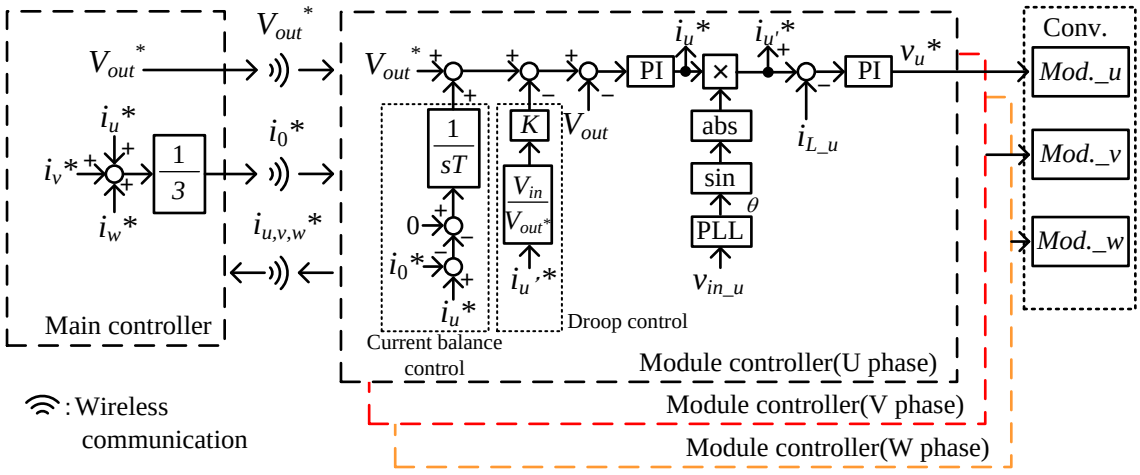

Fig. 2. Control block diagram of proposed circuit.

In AVR, the PI controller is applied in order to regulate the output voltage into the DC voltage reference value from the main controller. In the input current control, the power factor in the primary side is corrected. Consequently, the input current i_L flowing through the boost inductor is controlled into full-wave rectification waveform. The current reference values $i_{Lu,\,v,\,w}$* are given by

$$i_{Lu,v,w}{}^{*} = I_{amp}\left|\sin(\omega t)\right| \qquad (2),$$

where I_{amp} is the amplitude of the reference. The phase information is obtained by detecting the input voltage. The response of AVR is designed to be sufficiently slow in comparison with ACR.

Hence, the gain of ACR is assumed as one, and the control interference is avoided. In addition, since the input current is feed-back in each individual phase, interference in control with other phases does not occur.

2.3. Droop control

In actual system is inevitable that error occurs in the detection gain due to the sensor. The unbalance of output current causes rush current when the potential difference occurs in the output voltage of each phase due to parallel connection of each phase. Therefore, in this proposed system, the droop control is applied to each module controller in order to eliminate rush current. The droop control is operated by dropping the dc voltage reference value according to the droop gain K in order to make the voltage gain within the range of the droop gain K.

Figure 3 shows an equivalent circuit of the droop control when the gain K is regarded as the virtual resistance R_K. On the other hand, the rush current is suppressed by regarding the droop gain K as the virtual resistance when the droop control is applied. The current of each phase i_x is introduced by (3) using the virtual resistance R_K,

$$\begin{aligned} i_x &= -\frac{1}{R_K}\left[\left\{\frac{R_{out}\left(V_{out\_u}+V_{out\_v}+V_{out\_w}\right)}{3R_{out}+R_K}\right\}-V_{out\_x}\right] \\ &= -\frac{1}{R_K}\left(V_{out}-V_{out\_x}\right) \\ &\left(x=u,v,w\right) \end{aligned} \qquad (3),$$

where R_{out} ,V_{out} and V_{out_x} are the load resistance, the summation of the output voltages of all three phases and the output voltage of each phase including the error. According to (3), as the droop gain increases, the output voltage V_{out} decreases in proportion to the virtual resistance R_K. In order to control without divergence, the current of each phase i_x must be larger or equal to zero because the droop control is not established. In other words, if the output voltage of each phase becomes larger than the output voltage, control does not diverge. Therefore, the divergence is suppressed by setting the droop gain higher than a predicted error. For example, the divergence is suppressed by designing the droop gain higher than the nominal error of the voltage sensor.

Since the amplitude of the input current is determined by the detection voltage and the droop gain with the droop control, the current amplitude differs between each phase; therefore, the current balance control is required.

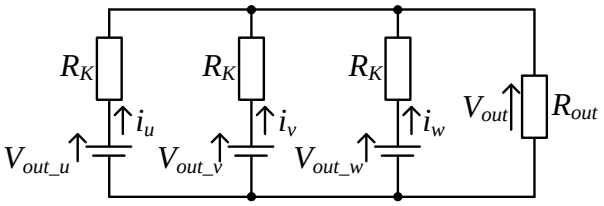

Fig. 3. Equivalent circuit of droop control.

2.4. Current balance control

The unbalance of each current is not eliminated although the droop control is applied because the droop control is suppressed divergence. Therefore, the unbalance of each current is suppressed by applying current balance control. As shown in Fig. 2, the direct current reference value of each phase is calculated in the main controller. Then, the averaged DC reference value i_0* and the DC current reference values $i_{u,\,v,\,w}$* of each phase are computed in the module controller to generate deviation. Then, this deviation is feed-back to the voltage reference value of each phase to eliminate the deviation between the direct current reference value i_0* and the direct current reference value of each phase $i_{u,v,w}$*.

Consequently, the current of each phase is balanced. The average value of the direct current reference i_0* is given by

$$i_0 = \frac{i_u^* + i_v^* + i_w^*}{3} \qquad (4).$$

In the conventional balance control, the main controller directly controls the current reference value. Therefore, it is necessary to increase fast response until that there is no influence on the voltage control among the centralized controller and module controller. This results in requirements of fast response main controller, and high-speed. Thus, the wireless communication is not implemented. In contrast, since the proposed control is controlled by the outer loop of the voltage control, lower response is acceptable in comparison with the voltage control.

As a result, the proposed system does not require fast or high-speed communication between the main controller and the module controller. This enables the employment of the wireless communication instead of the wired communication.

3. SIMULATION RESULT

In this section, the effectiveness of the current balance control is confirmed with simulation. Table I shows simulation conditions. In Fig. 1, each phase is composed of multiplicity of modules. In this consideration the number of the module on each phase is one for simplicity.

As mentioned in section 2, since the current reference of ACR as full-wave rectification waveform has the frequency components of the twice the grid frequency, i.e. 100 Hz or 120 Hz fast response ACR is required. The angular frequency is 628 rad/s when the grid frequency is 50 Hz. Therefore, in this simulation, the angular cut-off frequency of ACR is designed to 6000 rad/s which is about 20 times angular grid frequency.

Besides, the angular cut-off frequency of AVR is designed to 50 rad/s because the reference value is direct current; therefore, response is not required. The rated capacity of the system is 150 kW, and the input voltage is 400 V. In order to simulate the detection error of the output voltage, the detection value of the output voltage of U phase is decreased by 5% on purpose. Furthermore, the integration time of current balance control is 0.1 s, which is slower than the response of the voltage control.

Figure 4 shows simulation results when only the droop control is applied, and when both the droop control and the current balance control are applied. It is seen that the power factor of the input current is almost unity.

In the case of the application of only the droop control, the current imbalance rate is 49.4%. On the other hand, the current imbalance rate is reduced to 0.1% when both the droop control and the current balance control are employed. Therefore, it is confirmed that the imbalance of the current is reduced compared with the case of the application of only the droop control. In addition, the input current THD is 0.09%. The output voltage is 491 V with a reference value of 500 V.

Table 1. Simulation condition.

Input voltage	v_{in}	400 V
Rated power	P	150 kW
Conveter capcitance	C_{conv}	1000 μF
Output capcitance	C_{out}	680 μF
Input inductance	L	7 μH
Load resistance	R_L	1.67 Ω
Voltage reference	V_{dc}*	500 V
Switching frequency (PFC)	f_{sw}	20 kHz
Resonant frequency (Resonant DC-DC converter)	f_o	50 kHz
Angular frequency of ACR	ω_{ACR}	6000 rad/s
Angular frequency of AVR	ω_{AVR}	50 rad/s
Droop gain	K	0.10p.u.
Trans turns ratio	N_1:N_2	1.0

4. EXPERIMENTAL RESULT

In this section, the operation of the circuit with both combination of the droop control and the current balance control is confirmed. Table II shows specifications and experimental conditions.

In Fig. 1, each phase is composed of multiplicity of modules, but in the experiment, it is composed of one module. In order to

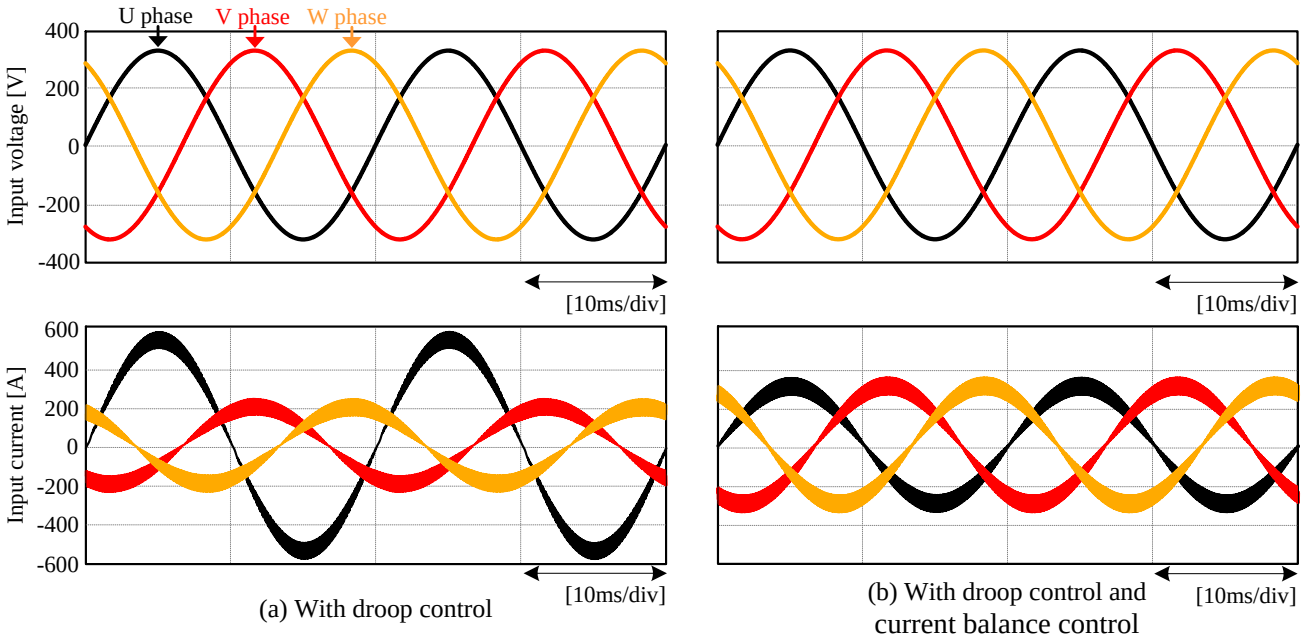

Fig. 4. Waveforms of input voltage, input current and output voltage.

confirm the effect of the proposed control, the output voltage detection value of the U phase was decreased by 10% on purpose, and the droop gain was set to 0.15 p.u.

Figure 5 (a) shows the input current waveform before application of proposed control. It is confirmed from Fig. 5 (a) that the input current is the unbalanced and it has distortion when the voltage detection gain is unbalanced.

Figure 5 (b) shows the input current waveform of each phase with the proposed control. As shown in Fig. 5 (b), the input current amplitude of each phase is almost same among each module and the current balance control is in operation. The ripple superimposed on the current amplitude is generated by the grid interconnection filter. Also, the current imbalance rates is 0.46%.

Table 2. Experimental condition.

Input voltage	v_{in}	200 V
Rated power	P	330 W
Conveter capcitance	C_{conv}	48 μF
Output capcitance	C_{out}	680 μF
Input inductance	L	7 mH
Load resistance	R_L	120 Ω
Voltage reference	V_{dc}*	200 V
Switching frequency (PFC)	f_{sw}	20 kHz
Resonant frequency (Resonant DC-DC converter)	f_o	50 kHz
Angular frequency of ACR	ω_{ACR}	6000 rad/s
Angular frequency of AVR	ω_{AVR}	50 rad/s
Droop gain	K	0.15p.u.
Trans turns ratio	N_1:N_2	1.0

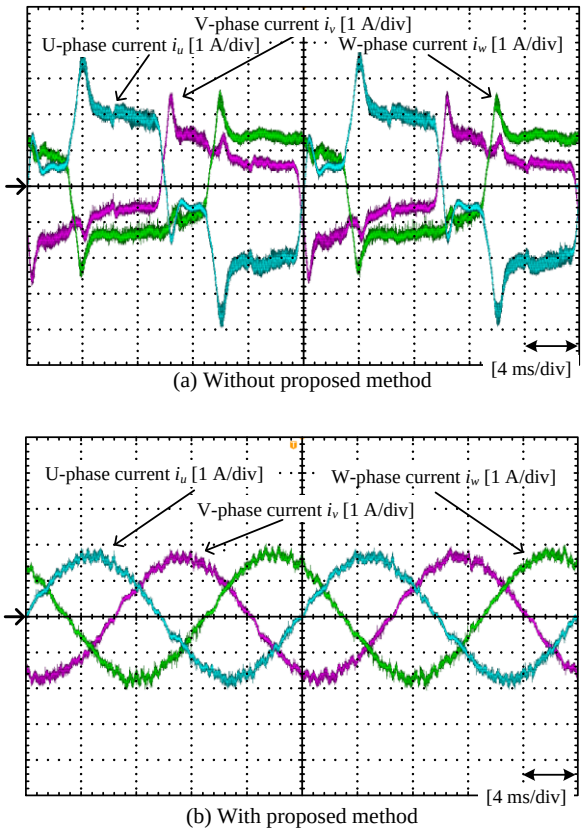

Fig. 5. Grid current waveforms

The difference in the current amplitude in each phase is caused by error of the detection gain.

It is confirmed that it is controlled without divergence by the proposed control. Then, the input current THD of each phase is

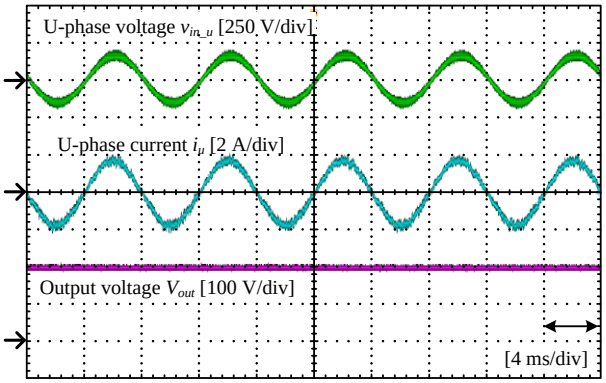

Fig. 6. U-phase waveforms of input voltage, input current and output voltage.

2.97% for U phase, 2.33% for V phase and 2.36% W phase. Figure 6 shows the U-phase input voltage, input current and output voltage waveform. From Fig. 6, the input current of the U phase is a sinusoidal. Moreover, and power factor is unity. In addition, the average value of the output voltage is 206 V, which is almost equal to the reference value 200 V. It is confirmed that it is operate satisfactorily. The output voltage is higher than the reference value owing to the effect of the droop gain.

Figure 7 shows the transient response of the input current when the load resistance value is stepped from 0.5 p.u. to 1.0 p.u.. From Fig. 7 it is confirmed that even in the case where the voltage detection gain is unbalanced. In the steady state, the gain is controlled in the same way as when the gain is in the equilibrium state. Then the average value of the output voltage is almost equal to the reference value when load resistance value is changed. Finally, the error between the voltage command and the detection votage is compensated control. This is because the detection gain is adjusted by the droop control and the current balance control.

Figure 8 shows the output voltage and the DC-link voltage of each phase. The resonance DC-DC converter is driven by open loop with a duty ratio of 50%. Also, the DC-link voltage is twice the output voltage. As shown in Fig. 8, the unbalance rates of the DC-link voltage average values are 0.47% when the detection error ratio is zero. In other words the output voltage becomes constant by the proposed control. Also, the unbalance rate of the average value of DC-link voltage is 0.45% when the detection error ratio is 10%. DC-link voltage is the same value as when the gain was balanced, and it was confirmed that it was well controlled.

Also, since each phase operates as a single-phase PFC circuit, pulsating current of twice the frequency of the system frequency occurs in the DC-link voltage. Since the output of modules are connected in parallel, the pulsating flows cancel each other and only the DC component is obtained.

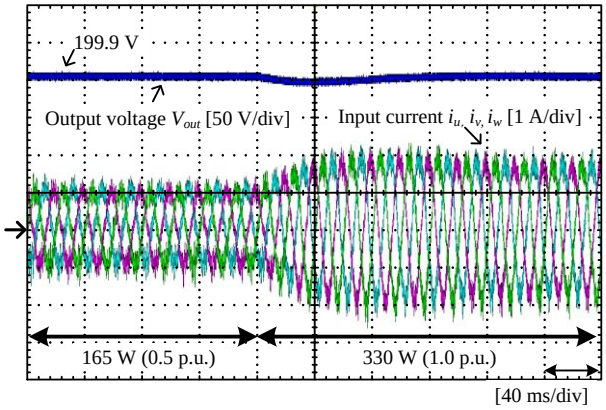

(a) detection error = 0%

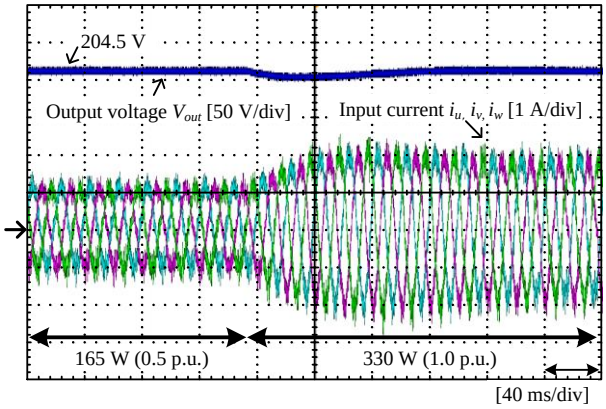

(b) detection error = 10%

Fig. 7. Step response of output voltage and input current.

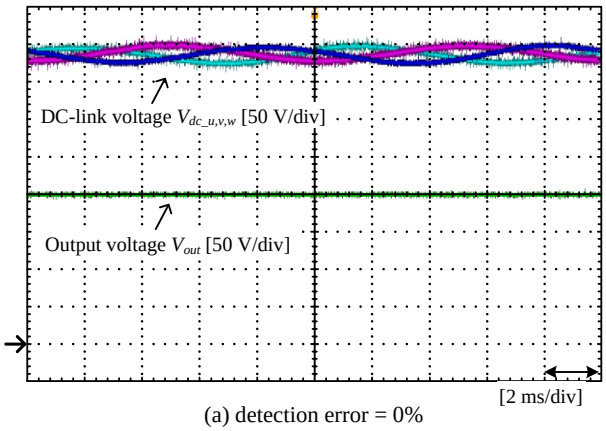

(a) detection error = 0%

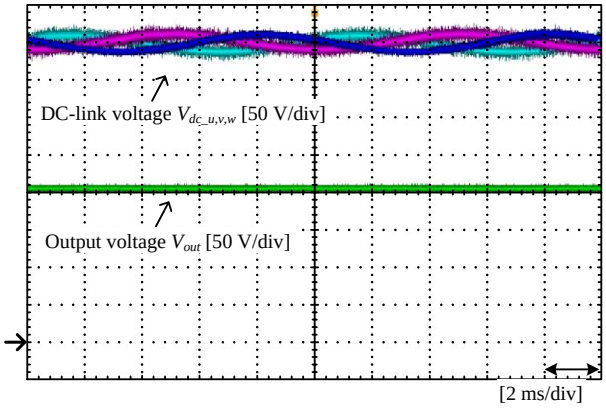

(b) detection error = 10%

Fig. 8. Waveform of output voltage and DC-link voltage.

5. CONCLUSION

This paper proposes an autonomous distributed control method for an isolated three-phase AC-DC converter in which a controller is included in each module. In the conventional multi-module topology, fast response is required for the main controller because the balance control among the modules is required. In contrast, by applying the droop control and the current balance control, it is achieved to balance the modules without fast response on the main controller in the proposed control scheme. The simulation results shows that there is a problem that the input current amplitude is unbalanced only by droop control when gain unbalance occurs. However, the input current imbalance rate is reduced from 49.4% to 0.1% by combining the current balance control and the droop control. Moreover, the experiments were carried out using a scaled model. As a result, it is confirmed that the input current of each phase is controlled to be sinusoidal and unity power factor is achieved. In addition, since the output voltage also follows the reference value with an error of 2.95%.

REFERENCES

(1) J. Teng, S. Liao, C. Wen: "Design of a Fully Decentralized Controlled Electric Vehicle Charger for Mitigating Charging Impact on Power Grids", IEEE Transactions on Industry Applications, Volume: 53, Issue: 2, pp.1497-1505 (2017)

(2) J. Lu, A. Mallik, A. Khaligh: "Dynamic Strategy for Efficiency Estimation in a CCM-Operated Front-End PFC Converter for Electric Vehicle Onboard Charger", IEEE Transactions on Transportation Electrification, Volume: 3, Issue: 3, pp.545-553 (2017)

(3) A. Mallik, W. Ding, A. Khaligh: "A Comprehensive Design Approach to an EMI Filter for a 6-kW Three-Phase Boost Power Factor Correction Rectifier in Avionics Vehicular Systems", IEEE Transactions on Vehicular Technology, Volume: 66, Issue: 4, pp.2942-2951 (2017)

(4) D. Kim, M. Kim, B. Lee: "An Integrated Battery Charger With High Power Density and Efficiency for Electric Vehicles", IEEE Transactions on Power Electronics, Volume: 32, Issue: 6, pp.4553-4565 (2017)

(5) C. Saber, D. Labrousse, B. Revol, A. Gascher: "Challenges Facing PFC of a Single-Phase On-Board Charger for Electric Vehicles Based on a Current Source Active Rectifier Input Stage", IEEE Transactions on Power Electronics, Volume: 31, Issue: 9, pp.6192-6202 (2016)

(6) C. Li, W. Huang, R. Cao, F. Bu, Changxin Fan: "An Integrated Topology of Charger and Drive for Electric Buses", IEEE Transactions on Vehicular Technology, Volume: 65, Issue: 6, pp.4471-4479 (2016)

(7) K. Wada: "Further Evolution Towards a New Generation of Electric Vehicles i-MiEV", Journal of Asian Electric Vehcles, Vol.8, No.2, pp.1405-1408, (2010)

(8) M. Nakahara, and K. Wada: "Loss Analysis of Magnetic Components for a Solid-State-Transformer", IEEJ Journal of Industry Applications, Vol.4, No.7, pp.387-394, (2015)

(9) H. Chen, A. Prasai, R. Moghe, K. Chintakrinda, D. Divan: "A 50-kVA Three-Phase Solid-State Transformer Based on the Minimal Topology: Dyna-C", IEEE Transactions on Power Electronics., Vol.31, Issue.12, pp.8126-8137 (2016)

(10) J. Itoh, K. Aoyagi, K. Kusaka, M. Adachi: "Single-phase Solid-State Transformer Using Multi-cell with Automatic Capacitor Voltage Balance Capability" The 2018 International Power Electronics Conference, Niigata, pp.2237-2244 (2018),

(11) X. Yu, X, She, X. Zhou and A. Q. Huang: "Power Management for DC Microgrid Enabled by Solid-State Transformer", IEEE Trans., Vol.5, No.2, pp.954-965 (2014)

(12) X. Wang, J. Liu, S. Ouyang, T. Xu, F. Meng, S. Song: "Control and Experiment of an H-Bridge-Based Three-Phase Three-Stage Modular Power Electronic Transformer", IEEE Transactions on Power Electronics, Volume: 31, Issue: 3, pp.2202-2011 (2016)

(13) Y. Li, L. Fan: "Stability Analysis of Two Parallel Converters With Voltage–Current Droop Control", IEEE Transactions on Power Delivery, Volume: 32, Issue: 6, pp.2389-2397 (2017)

(14) N. F. Avila, C. Chu: "Distributed Pinning Droop Control in Isolated AC Microgrids", IEEE Transactions on Industry Applications, Volume: 53, Issue: 4, pp.3237-3249 (2017)

(15) X. Chen, L. Wang, H. Sun, Y. Chen: "Fuzzy Logic Based Adaptive Droop Control in Multiterminal HVDC for Wind Power Integration", IEEE Transactions on Energy Conversion, Volume: 32, Issue: 3, pp.1200-1208 (2017)